

Nature of metal-nonmetal transition in metal-ammonia solutions.

II. From uniform metallic state to inhomogeneous electronic microstructure

Gennady N. Chuev^{1*} and Pascal Quémerais²

⁽¹⁾ *Institute of Theoretical and Experimental Biophysics,*

Russian Academy of Science, Pushchino, Moscow Region, 142290, Russia

⁽²⁾ *Institut Néel, CNRS, BP 166, 38042 Grenoble Cedex 9, France*

(Dated: February 9, 2022)

Applying semi-analytical models of nonideal plasma, we evaluate the behavior of the metallic phase in metal-ammonia solutions (MAS). This behavior is mainly controlled by the degenerate electron gas, which remains stable down to 5 MPM due to high solvent polarizability and strong dielectric screening of solvated ions. Comparing the behavior of the metallic state with those of localized solvated electrons, we have estimated the miscibility gap Δn for various alkali metals and found $\Delta n(\text{Na}) > \Delta n(\text{K})$. It is rather narrow in Rb-NH₃ and does not occur in Cs-NH₃ solutions, which is in full agreement with the experiments. The case of Li is discussed separately. The difference calculated in the excess free energies of the metallic and nonmetallic phases is in the order of $k_B T$, yielding a thermally fluctuating mixed state at intermediate metal concentrations. It results in a continuous metal-nonmetal (MNM) transition above the consolute point T_c and a phase separation below T_c . We propose a criterion for the MNM transition which may be attributed to the line of the maximum of compressibility above T_c . This line crosses the spinodal one at the critical temperature. Finally, we assert that a new electronic phase similar to microemulsion should also arise between the spinodal and the binodal lines.

* e-mail addresses: genchuev@rambler.ru and pascal.quermerais@grenoble.cnrs.fr

I. INTRODUCTION

Metal-ammonia solutions (MAS) are an example of quantum-classical systems whose thermodynamic, dielectric, and optical properties are controlled by electron-electron interactions. In our recent papers^{1,2} we have explained that these interactions are mainly due to the dispersion attractions between solvated electrons at metal concentrations in the range of 1-5 MPM.³ These attractions result in two main effects: a phase separation in solutions of light alkali metals below a critical temperature, and a dielectric instability of the solution, which may be considered as the onset of metallization. Considering the role of the induced dipolar interactions between solvated electrons, we have restricted ourselves to the nonmetallic phase.² We have already given an indication¹ that the metal-nonmetallic (MNM) transition, or insulator-to-metal transition (IMT), are likely driven by a Goldhammer-Herzfeld (GH) mechanism,^{4,5} i.e. a polarization catastrophe which has its origin in the dispersion interactions. We have also indicated that the correlation effects¹ and the solvent polarizability⁶ may be responsible for the unusual properties of the metallic phase and lead to its instability at metal concentrations lower than 5 MPM. As explained in Ref.¹, this seems to forbid the Mott-like scenario for the MNM transition in MAS. That point reactivates the old debates of Mott,^{7,8,9} Jortner, and Cohen^{10,11,12} on the nature of the MNM transition. Mott assumed the phase separation to be a consequence of the Mott-like transition, which is hidden by the phase separation below the consolute temperature ($T < T_c$), and the MNM transition above the temperature ($T > T_c$) should be of the Anderson type due to disorder. On the contrary, Jortner and Cohen¹² described the system above the consolute point as a microscopically inhomogeneous regime in which the concentration fluctuates locally one of the other well-defined values M_0 and M_1 ($M_0 > M_1$), and the MNM mechanism does not involve the Mott transition. According to them, the concentration $M_1 \approx 2$ MPM corresponds to the nonmetallic blue phase (consisting of solvated electrons as described in Ref.^{1,2}), whereas the concentration $M_0 \approx 9$ MPM corresponds to the bronze metallic phase in which electrons are delocalized and move freely. Using this hypothesis and a semi-classical theory of percolation, Jortner and Cohen were able to account for most transport properties observed in the intermediate concentration regime above the consolute temperature.^{10,11,12} However, in the conclusive part of their paper,¹² they pointed out the four important unsolved questions: 1) 'what is the origin of this microscopically inhomogeneous state?'; 2) 'what is the origin

of the phase separation?'; 3) is there any link between the two phenomena?; and finally 4) 'what is the nature of the MNM transition?'. We have already partly answered the last question in our previous papers^{1,2}, and we now think that we are able to answer the three other ones, at least at a qualitative level at this stage of our theory. This will be the subject of the discussion of the present paper, but we are mainly facing a new theoretical situation. Our results show that at low temperatures an intermediate concentration range exists in which both states, i.e., the nonmetallic one (the blue phase) and the metallic one (the bronze phase), are intrinsically unstable.^{1,2} Such a theoretical possibility has been already suggested by one of us^{13,14,15}. As we will discuss in this paper, we believe that this is at the origin of the phase separation, and that the existence of an inhomogeneous state above the consolute temperature should additionally be clarified.

There are numerous experimental data on the electronic^{16,17,18,19,20} and structural^{21,22,23,24,25} properties of the metallic state of MAS, but a theoretical treatment of concentrated MAS is restricted to a few papers only.^{10,11,26,27,28,29} The difficulty of such a treatment is twofold: first, the electron density in the metallic phase is still rather low so that strong electronic correlation effects occur, and, secondly, the molecular nature of the solvent as well as the sufficient role of the solvent polarizability complicate the theoretical study of these correlations in the metallic phase. The aim of the present work is to develop a statistical model treating the excess electrons in MAS under conditions corresponding to the metallic phase. This phase represents a three-component mixture consisting of delocalized electrons, cations, and polarizable solvent molecules. In general, a detailed information about electronic and thermodynamic properties of the system may be obtained by quantum molecular simulations based on the Car-Parrinello method.^{29,30,31,32} However, the computational costs and sensitivity of such calculations to the choice of the interaction potentials (an explicit account of cations, polarizability of solvent and so on) restrict the application of the method and cannot be used efficiently for a complete understanding of the phase behavior of MAS. An alternative way may be an employment of the integral equations theory based on quantum hypernetted chain closure³³, but the current status of such an approach is limited only to simple metals³⁴ or electrons localized in polar liquids^{35,36} and ionic liquids.^{37,38} Indeed, we do not know any applications extended to molecular metallic fluids. In order to avoid the complexity related to numerical implementations, we consider in the present paper that the metallic phase is well described

by an effective two-component plasma (TCP), where the role of the solvent is restricted to its screening effects. We take into account different frequency scales of this screening as we have done for the nonmetallic phase,^{1,2} i.e. that the screening of electron-electron interactions is due to the electronic polarizability of solvent, whereas ion-ion interactions are additionally screened by the permanent dipoles of the solvent molecules. As a result, we use different dielectric constants to treat the Coulomb interactions properly, i.e. a high-frequency dielectric constant for the electron-electron interactions and a low-frequency dielectric constant for ion-ion interactions respectively. By using available analytical expressions for the free-energy of the TCP^{39,40}, we will derive the main thermodynamic and dielectric characteristics of the metallic phase, its pressure and chemical potential, and we will evaluate the locus of the critical lines (spinodal and coexistence line) which correspond to the instability of the metallic phase. Then, by comparing the thermodynamic behavior of the metallic phase with that of the nonmetallic phase,^{1,2} we will give evidence that an inhomogeneous electronic microstructure must arise at intermediate metal concentrations in MAS. Although the detailed study of the inhomogeneous microstructure will be the subject of our next paper,⁴¹ we will assert in this work that the thermodynamic and dielectric peculiarities of the inhomogeneous electronic state govern the behavior of MAS in this concentration range. Eventually, by treating the inhomogeneous microstructure within the methods of simple liquids, we will propose a macroscopic criterion for the MNM transition, and sketch the complete phase diagram of MAS. Atomic units are used throughout.

II. MODEL

A. General outline.

The high-density phases of MAS are composed of delocalized interacting electrons scattered by ammonia molecules and solvated ions. As explained above, the solvent molecules are considered to result in the screening of the ions and the electrons only. The ion-ion interactions will be screened by the low frequency dielectric constant ϵ_l , while the electron-electron interactions will be screened only by the high frequency dielectric constant ϵ_h . Next we treat the system as a TCP, the first component being the interacting electron gas in a jellium, and the second component being a classical plasma of ions in a jellium of electrons.

Finally, we add an interaction term which represents a correction to the Madelung energy of the point ions in the jellium of electrons, i.e. a pseudo-potential correction due to the short-range scattering of the free electrons by valence core electrons of the ions. Notice that these ions are themselves solvated by ammonia molecules. This defines two different effective radii for the ions. The first one is an effective classical radius of the solvated ions, that we call r_{vdW} , which will be used to account for the classical short-range ion-ion interactions through the use of a packing factor. The second effective radius concerns the electron-ion interactions and it is related to the core ion radius, and we call it r_i . It includes the effect of the solvation shell of a particular ion. For alkali metals such as Na, K, Rb, Cs, the effective core radii are only slightly different from those determined by the pseudo-potential method⁴² for non solvated ions. However, the case of Li^+ is special, since it is well established²² that owing to their small size, the Li^+ ions occupy tetrahedral vacancies formed exactly by four ammonia molecules. From this point of view, Li^+ ions are strongly bound to form complexes $\text{Li}(\text{NH}_3)_4^+$, which are dominant ionic species in the solution. Consequently the core radius of solvated Li^+ is substantially larger than in the case of liquid Li metal.

Thus, our model contains four parameters ϵ_l , ϵ_h , r_{vdW} , r_{ion} , in addition to the Wigner-Seitz parameter $r_s = \hbar^2/m_e^2(4\pi n/3)^{1/3}$, related to the metal density (or the density of electrons, since the alkali metals are monovalent). Finally, the excess free energy per electron of the metallic phase is written as the sum of three terms:

$$f_m(n, T) = e_{DEG}(n) + f_{OCP}(n, T) + f_{ei}(n), \quad (1)$$

where $e_{DEG}(n)$ is the free energy per electron of an interacting electron gas with density n , and $f_{OCP}(n, T)$ is that of a classical one-component plasma (OCP) of ions in a jellium of electrons. Finally, the last term $f_{ei}(n)$ represents the electron-ion interactions and will be treated in the framework of the pseudo-potential theory⁴². Notice that Ashcroft proposed a similar approach to the metallic phase,²⁸ except that he didn't used the different dielectric constants in his model.

B. Free-energy of the interacting electron gas

The electron gas may be parameterized by two dimensionless parameters³⁹: the electron coupling constant $\Gamma_e = \beta e^2(4\pi n/3)^{1/3}/\epsilon_h$, and the reduced temperature $\Theta =$

$2m/\hbar^2\beta(3\pi^2n)^{2/3}$, where β is the inverse temperature. m and e are the electron mass and charge, respectively. However one can easily check that $\Gamma_e \sim 100 \gg 1$ and $\Theta \sim 0.05 \ll 1$ under conditions corresponding to the metallic phase in MAS, and therefore the electron gas is degenerate and we can treat it at $T = 0K$. Its free energy may be parameterized by the single parameter, i.e. the effective Wigner-Seitz radius defined as $r_s^* = r_s/\epsilon_h$. Applying the conventional methods for the electron gas, we have:

$$\left(\frac{\epsilon_h^2\hbar^2}{me^4}\right)e_{DEG}(n) = \frac{1.105}{r_s^{*2}} - \frac{0.458}{r_s^*} + e_{cor}(r_s^*). \quad (2)$$

The first two terms are obtained by the usual Hartee-Fock approximation, and the last term is the correlation energy (beyond the Hartree-Fock approximation). In order to treat this correlation energy $e_{cor}(r_s^*)$, which is a smooth function of r_s^* , we have employed the result of the local density approximation parameterized in Ref.⁴³ by fitting quantum simulations:

$$e_{cor}(r_s^*) = \frac{\gamma_0}{1 + \gamma_1 r_s^{*1/2} + \gamma_2 r_s^*}, \quad (3)$$

where $\gamma_0 = -0.1423$, $\gamma_1 = 1.0529$, and $\gamma_2 = 0.3334$ are numerical parameters obtained from ref.⁴³. As we noticed in Ref.¹, the degenerate electron gas gives the main contribution to the total excess free energy $f_m(n, T)$ of the metallic phase.

C. The classical one-component plasma

The mean distance between ions exceeds 9 Å at metal concentrations of about 10 MPM, so short-range details of the ion-ion interactions can be ignored, and we may treat the ions as charged hard-spheres in the uniform jellium background. Thus, the excess free energy of ions is controlled by the two dimensionless parameters: the dimensionless ion coupling constant $\Gamma_i = \beta e^2(4\pi n/3)^{1/3}/\epsilon_l$, and the packing factor $\eta = \pi n\sigma^3/6$ in which $\sigma = 2r_{vdW}$ is the classical hard-sphere ion diameter. Simple evaluations show that the first parameter is of about 10 in the metallic Na-NH₃, and that the second one does not exceed 0.05 under the same conditions. Therefore the free energy f_{OCP} per ion may be written as

$$\beta f_{OCP} = [\ln(n\Lambda_i^3) - 1] + f_{hs}(\eta) + f_C(\Gamma_i), \quad (4)$$

where the first term is the ideal contribution, $\Lambda_i = (2\pi\beta/M_i)^{1/2}$ is the de Broglie length and M_i is the ion mass. The second term in (4) is the hard-sphere contribution, and the last

term is the contribution due to Coulomb interaction between ions. Analytical expressions for these contributions are well-known. The hard-sphere part is expressed as⁴⁴:

$$\beta f_{hs}(\eta) = \frac{\eta(4 - 3\eta)}{(1 - \eta)^2}. \quad (5)$$

According to Ref.⁴⁵, in which simulation data were fitted for various Γ_i in the range $1 < \Gamma_i < 160$, the electrostatic contribution can be approximately written as:

$$\beta f_C(\Gamma_i) = -0.897\Gamma_i + 3.620\Gamma_i^{1/4} - 0.758\Gamma_i^{-1/4} - 0.815 \ln \Gamma_i - 2.58. \quad (6)$$

The first term in this expression represents the Madelung energy and gives the most important contribution. The remaining terms are temperature-dependent corrections due to thermal motion of the ions.

D. Electron-ion interaction

The main difficulty is to evaluate $f_{ei}(n)$, because the bare ion-electron interaction is modified in the solution by the polarizability of the solvent. Moreover, the Madelung term in eq. (6) concerns the point ions. The correction to this approximation is well treated by the pseudo-potential model for simple metals⁴². In that point we follow the Ashcroft approach²⁸ and adapt the pseudo-potential model⁴² to our case. As a result, we write the electron-ion contribution (expressed in effective atomic units $me^4/\epsilon_h^2\hbar^2$) as:

$$\left(\frac{\hbar^2\epsilon_h^2}{me^4}\right) f_{ei}(n) = \frac{3r_i^{*2}}{2r_s^{*3}}, \quad (7)$$

where $r_i^* = r_i/\epsilon_h$ and the ion-core parameter r_i is related to the atomic number of the ion as discussed above. Notice that in our previous paper,¹ we took a slightly different notation and wrote $f_{ei}(n) = a_i n$, so that $a_i = 6\pi r_i^2$ to make the exact link with the present paper.

III. THERMODYNAMICAL PROPERTIES

Once we know the expression of the excess free energy f_m per electron, we can deduce the excess pressure Δp , the excess chemical potential $\Delta\mu$, and the excess compressibility κ as determined by the usual formulas:

$$\Delta p = n^2 \frac{\partial f_m}{\partial n}, \quad \Delta\mu = f_m + n \frac{\partial f_m}{\partial n}, \quad \kappa^{-1} = n \frac{\partial \Delta p}{\partial n}. \quad (8)$$

As discussed above, it may be checked that the degenerate electron gas (DEG) gives the main contribution to $f_m(n, T)$ at low temperatures, whereas the ionic contribution is only a correction. Our TCP model of the metallic phase of MAS depends on temperature and metal concentration and can be characterized by the four parameters: r_{vdW} , r_i , ϵ_l , and ϵ_h . As we will see, the value of the ionic mass M_i in (4) does not change the values of the density at which the metallic state becomes unstable.

Earlier on², we have determined the low-density spinodal line $n_s(T)$ above which the solvated electrons become thermodynamically unstable. Now we evaluate the high-density counterpart of the spinodal line $n_{c2}(T)$ corresponding to the zero derivative of the excess chemical potentials or the excess pressure:

$$\partial\Delta\mu/\partial n = \partial\Delta p/\partial n = 0. \quad (9)$$

Since the main part of the excess free energy in the metallic phase is coming from the degenerate electron gas, the high-density spinodal $n_{c2}(T)$ will depend weakly on temperature.

For any second-order phase transition there are two curves: the spinodal and the binodal ones, the last curve corresponds to the liquid-liquid coexistence. As we explained in Ref.², the low- and high-density spinodals are given by $n_s(T)$ and $n_{c2}(T)$, respectively. In principle, to calculate the coexistence curve, we need a complete knowledge of the excess free energy $f(n, T)$ in the whole range of density, which is beyond the current status of our theory. However, we may use the following argument to estimate the high-density part of the coexistence curve: the excess pressures of the low-density and high-density phases must be equal (this is the coexistence condition). But we know that the excess pressure of the low density phase is roughly close to zero (more exactly it is in the order of $nk_B T$),² whereas the excess pressure of the metallic phase strongly varies with n . Therefore, we assert that the coexistence curve $n_p(T)$ at high density will be roughly given by the condition:

$$\Delta p(n_p) = 0. \quad (10)$$

The critical concentration $n_{c2}(T)$ defines the low-density limit of the absolute stability of the metallic phase, whereas the critical concentration $n_p(T)$ is close to the line of liquid-liquid coexistence. The metallic phase cannot exist below $n_{c2}(T)$, and in the range $n_{c2}(T) \leq n \leq n_p(T)$ the solution is not homogeneous (the pressure becomes negative) and consists of domains of the metallic phase together with nonmetallic islands being nuclei of the low

density phase, i.e. the solvated electron phase. The uniform metallic phase remains stable for densities $n > n_p(T)$.

IV. THE USE OF EXPERIMENTAL DATA TO FIT THE MODEL PARAMETERS

Our input phenomenological parameters are r_i , r_{vdW} , ϵ_h , and ϵ_l . For the pure ammonia solvent, we take $\epsilon_\infty = 1.756$, $\epsilon_s(T = -70^\circ\text{C}) = 25$, and $\partial\epsilon_s/\partial T = -0.1 \text{ K}^{-1}$.⁴⁶ We use the data on the ammonia density,⁴⁷ namely, $n_{NH_3} = 0.0255\text{\AA}^{-3}$ at $T = -70^\circ\text{C}$. In order to take into account phenomenologically the influence of free electrons on the high-frequency dielectric constant, we apply:

$$\epsilon_h(n) = \epsilon_\infty - Ac, \quad (11)$$

where $c = n/(n + n_{NH_3})$ is the relative fraction of the metal in the solution, and A is a phenomenological parameter. In general, the low-frequency dielectric constant ϵ_l may deviate also from the bulk value ϵ_s due to saturation of orientational polarization in the vicinity of ions. Simple estimates show that the low-frequency constant can decrease down to 9.⁴⁸ Therefore, different values for ϵ_l could also be tested. The core-radii and van-der-Waals radii can be extracted from the literature, which we do in our first parameterization (model 1). However, as we discussed above, this does not take properly into account the fact that the ions are solvated. Then we propose a second procedure to evaluate these radii, that we call model 2.

Model 1. The ion-core radii r_i are obtained from the data on simple metals.⁴² Although we do not find suitable estimates of van-der-Waals radii r_{vdW} for ions solvated in ammonia, we have used those of hydrated ions, assuming that the solvation properties of water are not so different from those of ammonia. We take the values for r_{vdW} from Ref.⁴⁹. That gives the values reported in Table 1 (at the lines: model 1). Finally, in this first model, we apply the phenomenological parameter $A = 1 - \epsilon_\infty = 0.756$, that takes into account the volume fraction occupied by the metal as in Ref.⁵⁰.

Model 2. For this model, the phenomenological constant A is used as a fitting parameter of experimental data on plasmon excitation measured in Li-NH₃.^{19,27} It is experimentally found $\epsilon_h = 1.44$ at 20 MPM so that $A = 1.58$. As discussed above, the case of Li raises a question, since the core radii obtained from Ref.⁴² do not take into account the solvation shell

of the ion. We use r_i as a parameter to fit the experimental data on the phase coexistence, which is known for Na-NH₃, Li-NH₃, and K-NH₃ solutions.⁵¹ We fit these data by (10), and obtain the values for the effective ion-core radius. A similar method is often used to fit ion-core radii for simple liquid metals.⁵² Comparing r_i to r_{vdW} for model 1, we find a proportionality constant of about 3/2 for Na-NH₃. Then we use the same proportionality constant to deduce r_{vdW} from r_i for Li, K, and Rb, which gives the values reported in Table 1 (at lines: model 2).

Table 1. Parameters of the metal ions and the calculated critical densities for models 1 and 2.

	model 1				model 2			
ion	$r_i(\text{\AA})^{42}$	$r_{vdW}(\text{\AA})^{49}$	$n_s(MPM)$	$n_{c2}(MPM)$	$r_i(\text{\AA})$	$r_{vdW}(\text{\AA})$	$n_s(MPM)$	$n_{c2}(MPM)$
Li	0.761	1.33	1.1	7.1	1.25	1.88	1.72	3.8
Na	0.939	1.68	1.32	4.92	1.12	1.68	1.32	5.2
K	1.234	2.02	2.04	3.0	1.31	1.97	1.96	3.4
Rb	1.323	2.16	2.76	2.65	1.33	2.0	1.96	3.2
Cs	1.449	2.54	5.0	2.15				

V. ANALYSIS

A. Pure metallic phase

Using the formulas described above, we have calculated the excess chemical potential and the excess pressure for the metallic phase of Na-NH₃ solutions. Figure 1 shows the concentration dependencies of these thermodynamic characteristics at various temperatures for model 1. As can be seen, the chemical potential has the minimum at $n_{c2} \approx 5$ MPM and the pressure is negative below $n_{cp} = 9$ MPM at low temperatures. Therefore, the metallic phase is not stable at densities lower than n_{c2} . This instability results from Coulomb correlations between delocalized electrons, because the main contribution to this compressibility is due to the DEG. It is well known (see f.e.⁵³) that the compressibility of a pure DEG in jellium (without polarizable medium), becomes negative at $r_s \geq 5.24$ and its pressure is negative for $r_s \geq 4.18$, which would correspond to $n_{c2} = 30$ MPM and $n_p = 46$ MPM, respectively. These estimates are far from the experimental values in MAS, which clearly indicates that the high

solvent polarizability and strong dielectric screening of ions stabilize the DEG in MAS to lower metal concentrations. The temperature influence on the stability is due to the ionic contribution, and it is as small as it should be for a quantum phase transition. The critical concentration n_{c2} varies only from 5.5 to 4.5 MPM as the temperature changes by 100^0 C. The critical concentrations obtained are sensitive to the choice of the input parameters r_i , ϵ_s , and A . Figures 2-4 show the variations of these critical concentrations with respect to these parameters. A decreasing contribution of the solvent polarizability tends mainly to destabilize the metallic phase, since $n_{c2} \propto \epsilon_h^{-3}(n)$, and an increasing ion-core radius promotes the phase stability at lower densities.

In our theory, we can estimate the miscibility gap by considering the range between the critical lines obtained at low density $n_s(T)$ (our previous paper²) and the present calculations of $n_{c2}(T)$. Both the lines $n_s(T)$ and $n_{c2}(T)$ give the locus of the low- and high-density spinodals, while the range $n_s \leq n \leq n_{c2}$ correspond to the miscibility gap. The results calculated at $T = -70^0\text{C}$ are listed in Table 1. We find that the gap decreases monotonically as the ion size rises as it happens for simple metals and the gap disappears for heavy ions like Cs, which is experimentally confirmed.¹⁶ Although these qualitative predictions provide a correct trend for the miscibility gap versus the ion size, the estimates based on the ion-core parameter derived from the theory of simple metals⁴² (our model 1) do not yield accurate evaluations of the phase separation range in case of Li-NH₃. The reason of this discrepancy is a peculiarity of local microstructure around the solvated ions, as we discussed above. Namely, the size of the Li ion is small, and the coordination number for the solvated Li ions is small too in comparison to other ions. As a result, the delocalized electrons scatter on the solvated Li-NH₃ complexes rather than on the cores of Li ions, and the effective ion-core size deviates sufficiently from the value obtained for simple metals. This drawback disappears when we apply model 2 and use the data on r_i fitting the zero-pressure condition (10) at the coexistence line. The critical concentrations n_s and n_{c2} calculated in this manner correspond much better to the experimental data (see Table 1); in particular, they yield the correct trend in the range $\Delta n = n_{c2} - n_s$ of the phase separation, namely, $\Delta n(\text{Na}) > \Delta n(\text{Li}) > \Delta n(\text{K})$. Both models 1 and 2 also indicate the absence of the phase separation in Cs-NH₃ solutions, while our results for Rb-NH₃ solutions exhibit a possibility a phase separation for model 2 and absence for model 1. The experimental evidence of such separation is not clear. There is no visible phase separation like in the Li-NH₃ solutions,⁵¹ although the measurements

of conductivity⁵⁰ and X-ray scattering⁵⁴ indicate large fluctuations at $n_c \approx 4$ MPM and at temperatures close to $T_c = 197^0\text{K}$. Those fluctuations can be interpreted as an indirect evidence of a phase separation for Rb-NH₃ solutions in this range.^{50,54}

We have also evaluated the compressibility κ as a function of the metal concentration n in the framework of model 2. The inverse compressibility κ^{-1} calculated is shown in Fig. 5 together with the experimental data derived from the measurements of plasmon excitations²⁰ obtained for the metallic Na-NH₃ and Li-NH₃ solutions above the consolute point T_c . As can be seen, there is a qualitative agreement between the calculated and the experimental data. Both indicate that the inverse compressibility decreases as the metal concentration decreases. However, the theoretical evaluation gives a much higher compressibility than the experimental measurements at intermediate densities. The deviations are more pronounced as the concentration decreases. In our opinion, it is an indirect evidence of the formation of an inhomogeneous electronic state consisting of a microscopic mixture of delocalized and localized electrons, as will be discussed in Sec. VB.

Finally, with the use of the calculated compressibility we can evaluate the low-frequency dielectric response of the metallic state at small wave-vectors ($k \rightarrow 0$), since we have the limiting relation for this function, as it takes place for the usual electron gas:

$$\varepsilon(\omega \rightarrow 0, k \rightarrow 0) = \varepsilon_h(n) + \frac{q_{TF}^2 \kappa_{free}}{k^2 \kappa}, \quad (12)$$

where q_{TF} is the Thomas-Fermi screening wave vector equal to $2(3n/\pi)^{1/6}/a_0$ (a_0 being the Bohr radius), and $\kappa_{free} = (3/\pi^4 n)^{1/3}/n$ is the compressibility of the ideal Fermi gas. The function $\varepsilon^{-1}(k) = 1/\varepsilon(\omega = 0, k \rightarrow 0)$ is depicted in Fig. 6 at various metal concentrations. This function becomes negative at concentrations below $n_{c2}(T)$, which confirms that the region of phase separation is indeed a region where the static dielectric constant must be negative.^{14,15}

The experimental phase diagram of sodium-ammonia solutions^{51,55,56} together with the different calculated critical lines corresponding to various instabilities of the nonmetallic and the metallic phases are depicted in Fig. 7. The low-density and the high-density spinodals correspond to the critical lines $n_s(T)$ and $n_{c2}(T)$, respectively, and the line $n_{c1}(T)$ of polarization catastrophe (see paper²) gives the onset of the MNM transition. Although our calculations of critical lines roughly correspond to the experimental situation, the experimental coexistence line coincides with the theoretical zero-pressure line of the metallic

phase only at low temperatures and deviates significantly from it as the temperature rises. The situation is similar for the calculated low-density and high-density parts of the spinodal curve, they do not cross as they should at the consolute point $T = T_c$. Therefore, at this stage of the theory, our model of the uniform metallic state and the homogeneous phase of solvated electrons phase cannot explain all the peculiarities of the phase behavior of MAS, although it indicates the main features of this behavior, namely, the existence of a miscibility gap giving rise to a phase separation.

B. Thermally fluctuating inhomogeneous state

To qualitatively understand what happens in the intermediate region, we have calculated the difference $f_{nm} - f_m$ between the excess free energies of the nonmetallic and the metallic phases. Following our previous study,² the free energy per electron in the nonmetallic state can be expressed as:

$$f_{nm}(n) = \frac{9}{8r_e^2} - \left[\frac{1}{\epsilon_\infty} - \frac{1}{\epsilon_s} \right] \frac{1}{2r_e} + 4\pi C_S \lambda r_e^2 + \frac{4\pi C_V n_{NH_3} r_e^3}{3\beta} + \quad (13)$$

$$+ 2\beta^{-1} \left[\ln(n\Lambda_i^{3/2}\Lambda_e^{3/2}) - 1 + \frac{\eta_{nm}(4 - 3\eta_{nm})}{(1 - \eta_{nm})^2} \right] - \frac{2}{\epsilon_s[\sigma + \gamma^{-1}]} + \frac{\gamma^3}{3\pi n\beta} - \frac{C_\alpha n r_e^3}{\epsilon_\infty^2},$$

where C_V , C_S , and C_α are numerical coefficients that we have already discussed in Ref.² and related to the temperature- and concentration- dependencies of the radius $r_e(n, T)$ of the solvated electrons, $\Lambda_e = (2\pi\beta/M_e)^{1/2}$ is the de Broglie length for localized electrons, M_e is their effective (classical) mass, λ is the surface tension, and $\eta_{nm} = \pi n(r_e + r_{vDW})^3/3$ is an effective packing factor, that we take equal to the mean value between the solvated electron and ion diameters. Eventually, $\gamma = ([1 + (32\pi n/\epsilon_s)^{1/2}(r_e + r_{vDW})]^{1/2} - 1)/2(r_e + r_{vDW})$ is the inverse screening length. The first row of the expression yields the solvation free energy of noninteracting electrons, and the second row results from electron-electron interactions and includes short-range, electrostatic, and dispersion contributions, respectively. All these contributions are only corrections to the free-energy of the electron solvation energy.²

To calculate f_{nm} , we have used our model described in Ref.², namely: $C_k = 1.5$, $C_r \approx 1.25$, $C_S = 1$ and $C_V = 1.75$, $\lambda = 40$ dyn/cm, and we apply $C_\alpha = 0.14$ and $\Lambda_e = 0.27\text{\AA}$. The difference $\delta f(n) = f_{nm}(n) - f_m(n)$ is shown in Fig. 8a. The main point to underline is that their difference remains in the order of only a few $k_B T$ along the range of concentration 1-10 MPM, although the values of the free energies of the metallic and non-metallic state are

both in the order of -0.7 eV. We should emphasize that this is not by chance. By carefully examining (and simplifying) the energy of both the metallic and non-metallic states, we can indicate that the main part of the energies coming from the electronic part is roughly given by:

$$f_{nm} \approx \frac{1.12}{r_e^2} - \left(\frac{1}{\epsilon_\infty} - \frac{1}{\epsilon_s} \right) \frac{0.5}{r_e}, \quad f_m \approx \frac{1.1}{r_s^2} - \frac{0.46}{\epsilon_\infty r_s} + \frac{e_{cor}(r_s/\epsilon_\infty)}{\epsilon_\infty^2}, \quad (14)$$

where f_m stands for the metallic phase, and f_{nm} for the nonmetallic one. That clearly indicates a crossing between the two energies when r_s tends to r_e , which is in quantitative agreement with the results shown in Fig. 8a.

Consequently, the thermal fluctuations between these electronic states must play a central role at intermediate densities, in particular to allow the closure of the miscibility gap at the critical temperature T_c by a mixing entropy effect. The detailed calculations of the complete phase diagram, including the calculation of T_c will be reported in our future paper.⁴¹ However, at a qualitative level, we may say that above the critical temperature, the system should be a microscopic mixture of both states, which is highly thermally fluctuating and roughly described by the relative fractions $n_m = (1 + \exp[\beta(f_m(n) - f_{nm}(n))])^{-1}$ and $1 - n_m$ of electrons in the metallic and nonmetallic state respectively, as a function of the metal concentration. The calculated values of n_m are also shown in Fig. 8b for Na-NH₃ solutions at $T = 240^0$ K. They indicate that our initial criterion of metallization, i.e. the polarization catastrophe above $n_{c1}(T)^{1,2}$ is spread out above T_c and becomes a progressive MNM transition, which should take place around the density $n_{c1}(T)$. Another peculiarity of the MNM transition is the compressibility of the mixed state consisting of localized solvated electrons as well as delocalized free electrons. The line of maximum of compressibility (or minimum of the inverse compressibility) may well characterize the MNM transition. This is sketched on Fig. 9 by the total inverse compressibility of the mixture. The total compressibility is well given by the sum of the inverse compressibility for each species (solvated electrons and delocalized ones) at the respective densities $1 - n_m$ and n_m . At the same time, the dielectric constant remains finite at the line of the minimum inverse compressibility, although it rises sharply in the nonmetallic phase close to this line, as discussed in our previous paper². It is worth noting that the mixed state qualitatively described here, is of a new kind in condensed matter (to our knowledge), and really results from the competition, driven by strong thermal fluctuations, between the delocalized and the self-trapped quantum states.

The situation is more simple below T_c . There is a finite range of densities between the spinodal and binodal curves at each side of the phase diagram, where the minority phase may nucleate in the majority phase to form some kind of stable electronic microemulsion. This microemulsion phase would be characterized by a large variety of aggregates as reported in numerical simulations²⁹. At the same time, the solution is phase separated below the spinodal line to prevent negative compressibility. The Fig. 10 summarizes all these effects. The MNM transition may be assigned to the line of the minimum inverse compressibility which crosses the spinodal and coexistence lines at the critical point $n_c(T_c)$. A more detailed theory of all these effects will be proposed in our future publication as well as more precise calculations of the spinodal and coexistence lines⁴¹. We have only qualitatively discussed in this paragraph the main features of the phase diagram resulting from our model.

VI. CONCLUSION

Thus, using the methods of non ideal plasma, we have evaluated the behavior of the pure metallic phase in MAS. We have asserted that this behavior is mainly controlled by the state of degenerate electron gas. Due to high polarizability of ammonia and high dielectric screening of ions solvated in MAS, the gas remains stable up to values of r_s of about 11, which is quite different from simple metals where available values of r_s do not exceed 6. The pure metallic phase is unstable at metal concentrations lower than 5 MPM. Comparing this critical concentration n_{c2} with the critical concentration $n_s(T)$ corresponding to the van-der-Waals instability of solvated electrons, we have evaluated the range Δn of the phase separation and found it to be governed by the ion-core size, the range decreasing as the ion-core size rises. By evaluating the ion-core size with the use of the zero-pressure condition applied to the coexistence line, we have obtained the correct trend in the range of the phase separation, namely, $\Delta n(\text{Na}) > \Delta n(\text{Li}) > \Delta n(\text{K})$. The phase separation does not occur in Cs-NH₃ solutions and is rather narrow in the case of Rb-NH₃.

Comparing the calculated free energy of pure metallic and nonmetallic phases, we have asserted the difference between the energies to be small due to minor differences in the energy of polaron formation and that of electron gas at the stability boundary. This leads to a strong influence of thermal fluctuations on the nature of the MNM transition, which becomes continuous above the critical temperature T_c . A thermally fluctuating inhomogeneous elec-

tronic mixture arises. It modifies substantially the criterion for the MNM transition, because this transition should be attributed to the line of the minimum inverse compressibility or to the maximum scattering factor. This line is quite close to our previous estimates $n_{c1}(T)$ corresponding to the polarization catastrophe and divergent dielectric constant,² although the dielectric constant remains finite at temperatures exceeding T_c .

At the same time, the dielectric constant and the compressibility must be negative below the spinodal line. To avoid such negativity, the system macroscopically separates into the metallic and nonmetallic phases below the spinodal line. A new electronic state arises in the range restricted by the spinodal and the binodal lines. This state can be characterized as an electronic microemulsion. The locus of the critical point n_c and the spinodal line is determined by the thermodynamic behavior of microemulsion and will be the subject of our next study.⁴¹ Concerning the criterion for the MNM transition, we should note that it is quite different from the one for usual semiconductors⁵⁷ and indicates a sufficient role of thermal fluctuations in the mechanism of MNM transitions. On the other hand, the line of the minimum inverse compressibility always exists for the second order transitions in simple⁵⁸ and molecular⁵⁹ liquids as well as for self-assembled networks.⁶⁰ This line crosses the spinodal line at the critical point. That is the reason why the MNM transition couples with the phase separation in MAS.

Acknowledgments

GNCh thanks the Russian Foundation for Basic research for partial support of this work.

¹ G. N. Chuev and P. Quémerais, *C. R. Physique* **8**, 449 (2007).

² G. N. Chuev, P. Quémerais, and J. Crain, *J. Chem. Phys.* **127** (Iss. 22, in press) (2007).

³ Mole fraction is calculated as a ratio of moles of the metal and that of the solution, $1(\text{MPM}) \approx 2 \cdot 10^{20} \text{ cm}^{-3}$.

⁴ D. A. Goldhammer, *Dispersion und Absorption des Lichtes in ruhenden isotropen Koerpern; Theorie und ihre Folerungen (mi 28 Textfiguren)*. Leipzig, Berlin, Teubner (1913).

⁵ K. F. Herzfeld, *Phys. Rev.* **29**, 701 (1927).

⁶ G. N. Chuev and P. Quémerais, *J. Chem. Phys.* **127** (Iss. 23, in press) (2007).

- ⁷ N. F. Mott, *Metal-Insulator Transitions* (Taylor and Francis, London, 1974).
- ⁸ N. F. Mott, Phys. Rev. Lett. **31**, 466, (1973).
- ⁹ N. F. Mott, J. Phys. Chem. **79**, 2915 (1975).
- ¹⁰ J. Jortner and M. H. Cohen, J. Chem. Phys. **58**, 5170 (1973).
- ¹¹ J. Jortner and M. H. Cohen, J. Phys. Chem. **79**, 2900 (1975).
- ¹² J. Jortner and M. H. Cohen, Phys. Rev. B **13**, 1548 (1976).
- ¹³ P. Quémerais and S. Fratini, Mod. Phys. Lett. B **11**, 1303 (1997).
- ¹⁴ P. Quémerais, J. L. Raimbault, and S. Fratini, J. Phys. IV **12**, 227 (2002).
- ¹⁵ P. Quémerais and S. Fratini, in *Polarons in Bulk Materials and Systems with Reduced Dimensionality*, ed. G. Iadonisi, J. Ranninger, and G. de Filippis, (IOS Press, Amsterdam, 2006).
- ¹⁶ J. C. Thompson, *Electrons in Liquid Ammonia* (Oxford Univ. Press, London, 1976).
- ¹⁷ C. N. Burns, P. M. Platzman, H. Sinn, A. Aletas, and E. E. Alp, Phys. Rev. Lett. **86**, 2357 (2001).
- ¹⁸ C. N. Burns, P. Giura, A. Said, A. Shukla, G. Vanko, M. Tuel-Benckendorf, E. D. Isaacs, and P. M. Platzman, Phys. Rev. Lett. **89**, 236404 (2002).
- ¹⁹ C. A. Burns, P. Abbamonte, E. D. Isaacs, and P. Platzman, Phys. Rev. Lett. **83**, 2390 (1999).
- ²⁰ A. H. Said, C. N. Burns, E. E. Alp, H. Sinn, and A. Alatas, Phys. Rev. B **68**, 104302 (2003).
- ²¹ H. Thompson, N. T. Skipper, J. C. Wasse, W. S. Howells, M. Hamilton, and F. Fernandez-Alonso, J. Chem. Phys. **124**, 024501 (2006).
- ²² H. Thompson, J. C. Wasse, N. T. Skipper, S. Hayama, D. T. Bowron, and A. K. Soper, J. Am. Chem. Soc. **125**, 2572 (2003).
- ²³ H. Thompson, J. C. Wasse, N. T. Skipper, C. A. Howard, D. T. Bowron, and A. K. Soper, J. Phys.: Condens. Matter **16**, 5639 (2004).
- ²⁴ J. C. Wasse, S. Hyama, N. T. Skipper, D. Morrison, and D. T. Bowron, J. Phys. Chem. B **107**, 14452 (2003).
- ²⁵ C. A. Burns, H. Sinn, A. Alatas, E. E. Alp, and A. Said, J. Chem. Phys. **124**, 024720 (2006).
- ²⁶ J. Jortner, I. Webman, and M. H. Cohen, J. Chem. Phys. **64**, 2013 (1976).
- ²⁷ U. Pinsook and S. Hannongbua, J. Chem. Phys. **124**, 074702 (2006).
- ²⁸ N. W. Ashcroft, J. Phys. IV, **1**, 169 (1991).
- ²⁹ Z.-H. Deng, G. J. Martyna, and M. L. Klein, J. Chem. Phys. **100**, 7590 (1994).
- ³⁰ Z.-H. Deng, G. J. Martyna, and M. L. Klein, Phys. Rev. Lett. **68**, 2496 (1992).

- ³¹ G. J. Martyna, Z. Deng, and M. L. Klein, *J. Chem. Phys.* **98**, 555 (1993).
- ³² Z.-H. Deng, G. J. Martyna, and M. L. Klein, *Phys. Rev. Lett.* **73**, 267 (1993).
- ³³ J. Chihara, *Prog. Theor. Phys.* **59**, 76 (1978).
- ³⁴ J. A. Anta and A. A. Louis, *Phys. Rev. B* **61**, 11400 (2000).
- ³⁵ G. N. Chuev, M. V. Fedorov, and N. Russo, *Phys. Rev. B* **67**, 125103 (2003).
- ³⁶ G. N. Chuev and N. Russo, *Chem. Phys. Lett.* **368**, 53 (2003).
- ³⁷ G. N. Chuev and V. V. Sychyov, *J. Chem. Phys.* **112**, 4707 (2000).
- ³⁸ G. N. Chuev, V. V. Sychyov, and O. Yu. Sokolova, *Phys. Rev. E* **63**, 061204 (2001).
- ³⁹ S. Ichimaru, *Rev. Mod. Phys.* **54**, 1015 (1982).
- ⁴⁰ S. Ichimaru, H. Iyetomi, and S. Tanaka, *Phys. Rep.* **149**, 92 (1987).
- ⁴¹ G. N. Chuev and P. Quémerais, *J. Chem. Phys.* (to be submitted) (2008).
- ⁴² C. Fiolhais, J. P. Perdew, S. Q. Armster, J. M. MacLaren, and M. Brajczewska, *Phys. Rev. B* **51**, 14001 (1995); *ibid* **53**, 13193 (1996).
- ⁴³ J. P. Perdew and A. Zunger, *Phys. Rev. B* **23**, 5048 (1981).
- ⁴⁴ N. F. Carnahan and K. E. Starling, *J. Chem. Phys.* **51**, 635 (1969).
- ⁴⁵ W. L. Slattery, G. D. Doolen, and H. E. DeWitt, *Phys. Rev. A* **21**, 2087 (1980).
- ⁴⁶ G. Billaud and A. Demortier, *J. Phys. Chem.* **79**, 3053 (1975).
- ⁴⁷ *Tables of Thermodynamic Properties of Ammonia*. (NBS, Circular 142, 1923).
- ⁴⁸ A. A. Likalter, *JETP* **84**, 516 (1997).
- ⁴⁹ W. L. Jorgensen, J. P. Ulmschneider, and J. Tirado-Rives, *J. Phys. Chem. B* **108**, 16264 (2004).
- ⁵⁰ J. A. Vanderhoff, E. W. LeMaster, W. H. McKnight, J. C. Thompson, and P. R. Antoniewicz, *Phys. Rev. A* **4**, 427 (1971).
- ⁵¹ P. D. Schettler and A. Patterson, *J. Phys. Chem.* **68**, 2865 (1964).
- ⁵² N. W. Ashcroft and D. C. Langreth, *Phys. Rev.* **155**, 682 (1967).
- ⁵³ S. Tanaka and S. Ichimaru, *Phys. Rev. B* **39**, 1036 (1989).
- ⁵⁴ J. V. Acrivos, K. Hathaway, A. Robertson, A. Thompson, and M. P. Klein, *J. Phys. Chem.* **84**, 1206 (1980).
- ⁵⁵ C. A. Kraus, *J. Am. Chem. Soc.* **29**, 1557 (1907).
- ⁵⁶ P. Chieux, and M. J. Sienko, *J. Chem. Phys.* **53**, 566 (1970).
- ⁵⁷ N. F. Mott, *Proc. Phys. Soc. A* **62**, 416 (1949).
- ⁵⁸ G. N. Sarkisov, *J. Chem. Phys.* **119**, 373 (2003).

- ⁵⁹ L. Xu, P. Kumar, S. V. Buldyrev, S.-H. Chen, P. H. Poole, F. Sciortino, and H. E. Stanley, Proc. Natl. Acad. Sci. **102**, 16558 (2005).
- ⁶⁰ A. G. Zilman and S. A. Safran, Phys. Rev. E **66**, 051107 (2002).

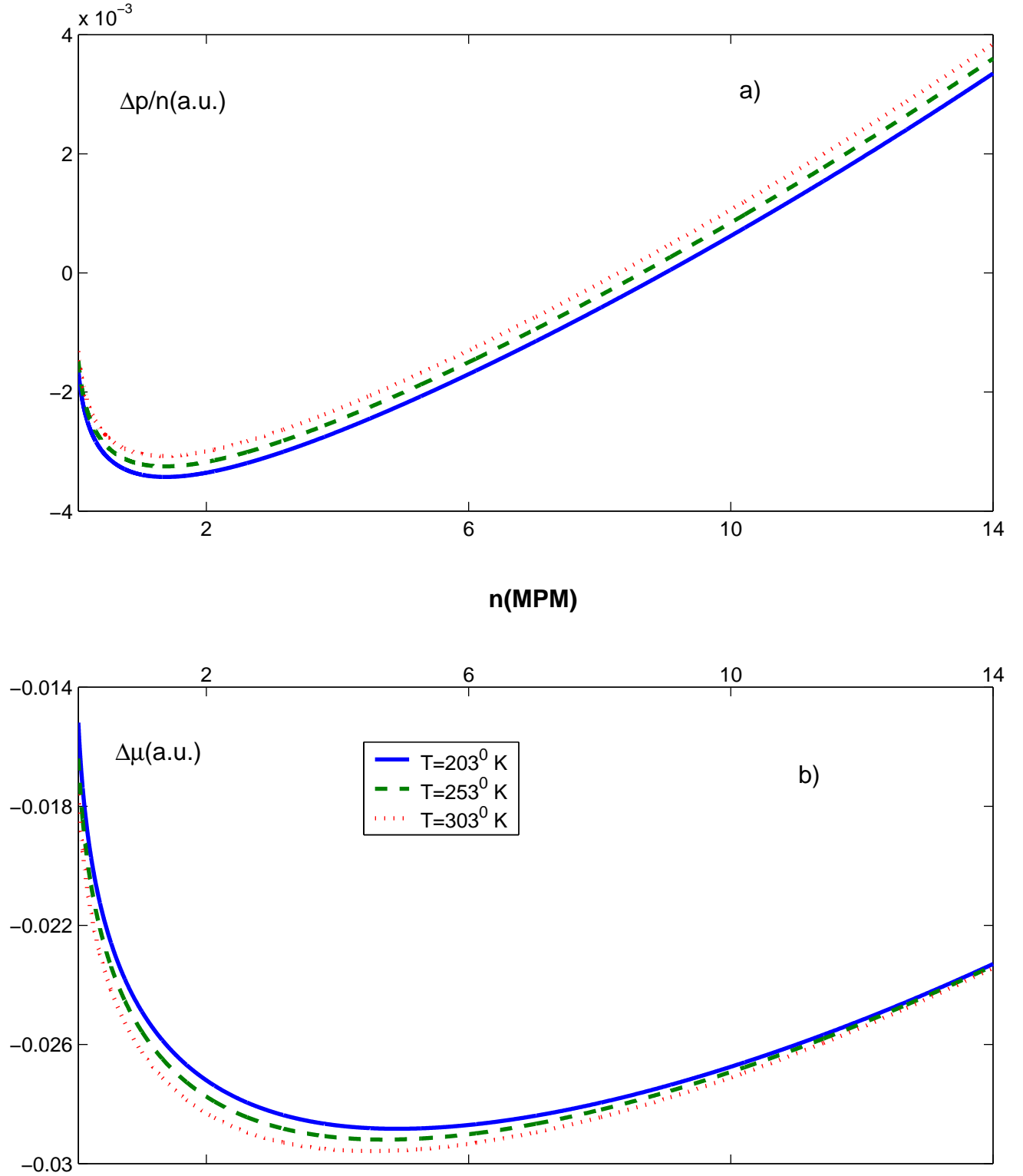


FIG. 1: The excess pressure $\Delta p(n, T)/n$ (a) and the excess chemical potential $\Delta\mu(n)$ (b) versus metal concentration n at various temperatures for the metallic phase of Na-NH₃ solution (model 1).

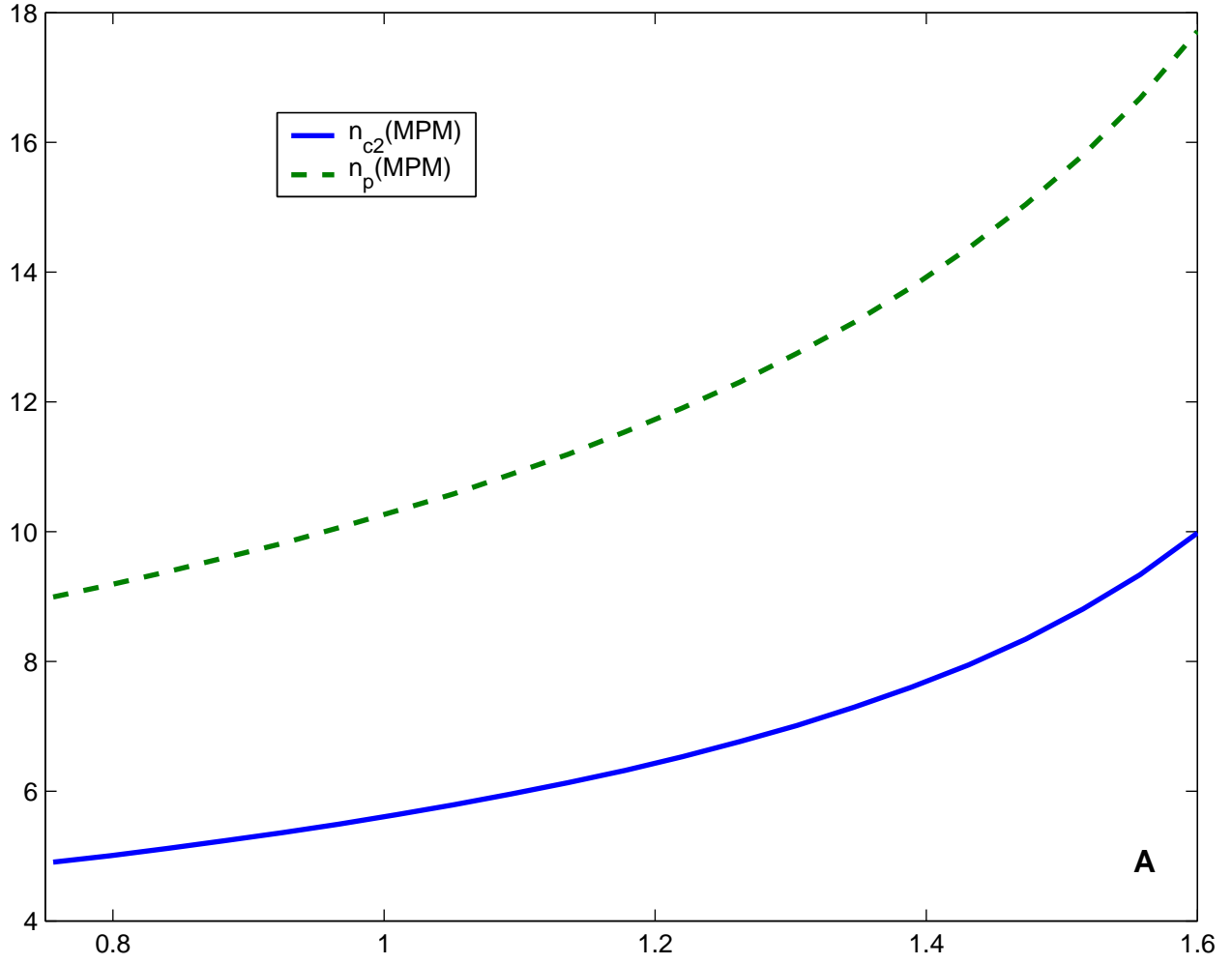


FIG. 2: Critical concentrations n_{c2} and n_p versus the parameter A for the metallic phase of Na-NH₃ at $T = -70^{\circ}\text{C}$ (model 1).

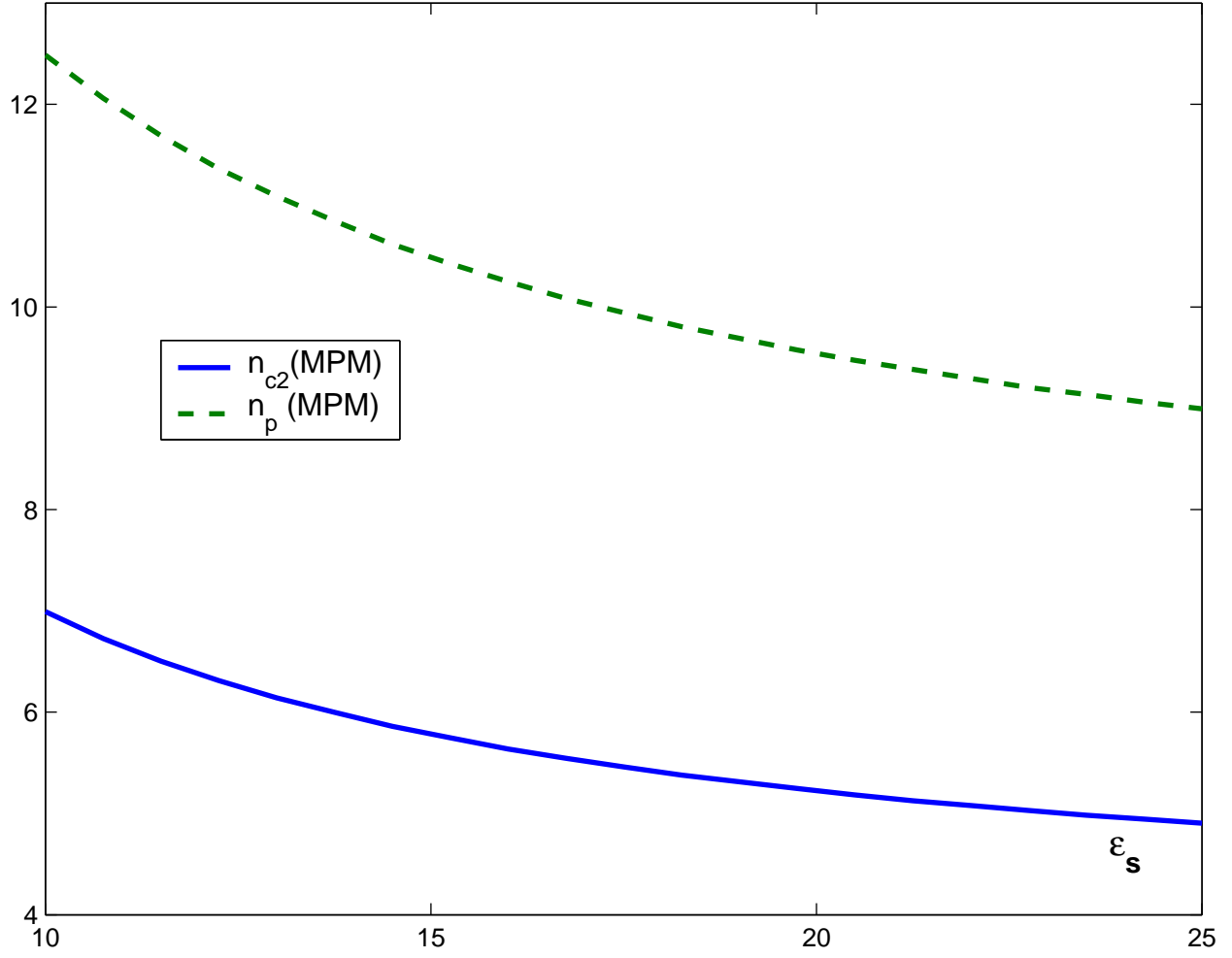


FIG. 3: Critical concentrations n_{c2} and n_p versus low-frequency dielectric constant ϵ_s for the metallic phase of Na-NH₃ at $T = -70^\circ\text{C}$ (model 1).

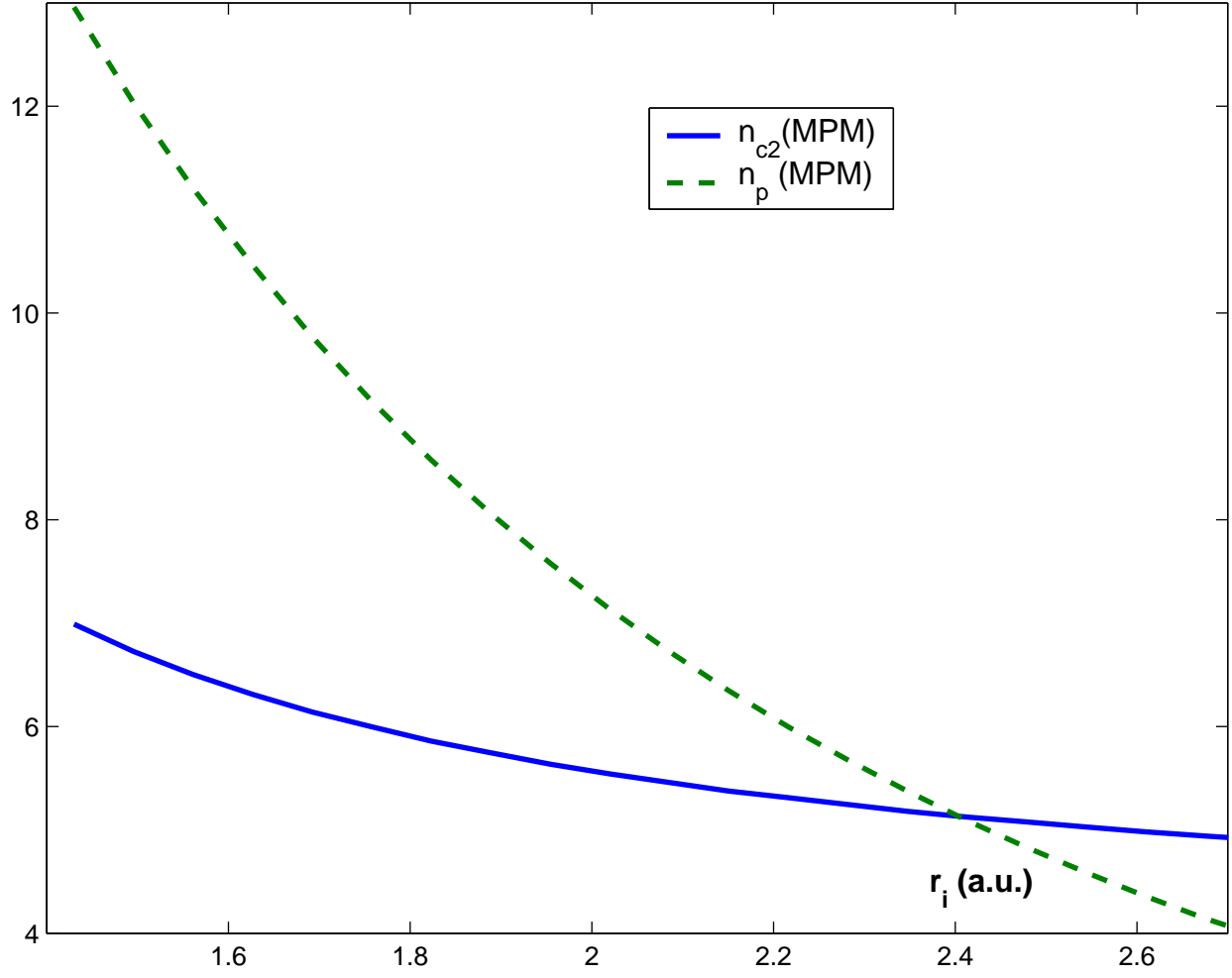


FIG. 4: Influence of the ion-core radius on the critical concentrations n_{c2} and n_p in the case of the metallic phase of Na-NH₃ at $T = -70^{\circ}\text{C}$ (model 1).

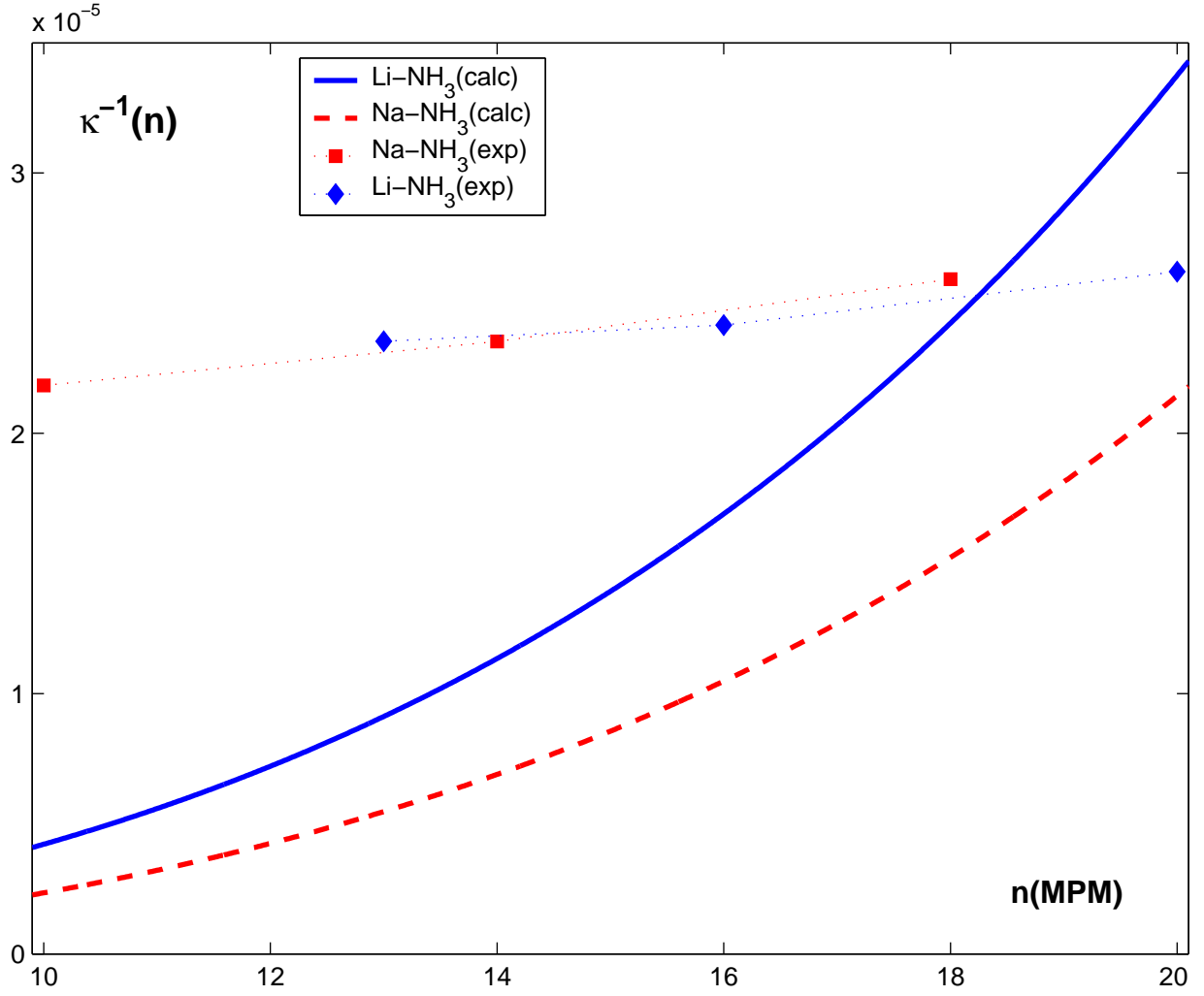


FIG. 5: The concentration dependence of the inverse compressibility κ^{-1} in MAS at $T = 240^0$ K. The solid curve indicates our calculations in the case of Li-NH₃ (model 2), and the diamonds are the experimental data from²⁰, the dashed curve and the squares are the same in the case of Na-NH₃ solutions.

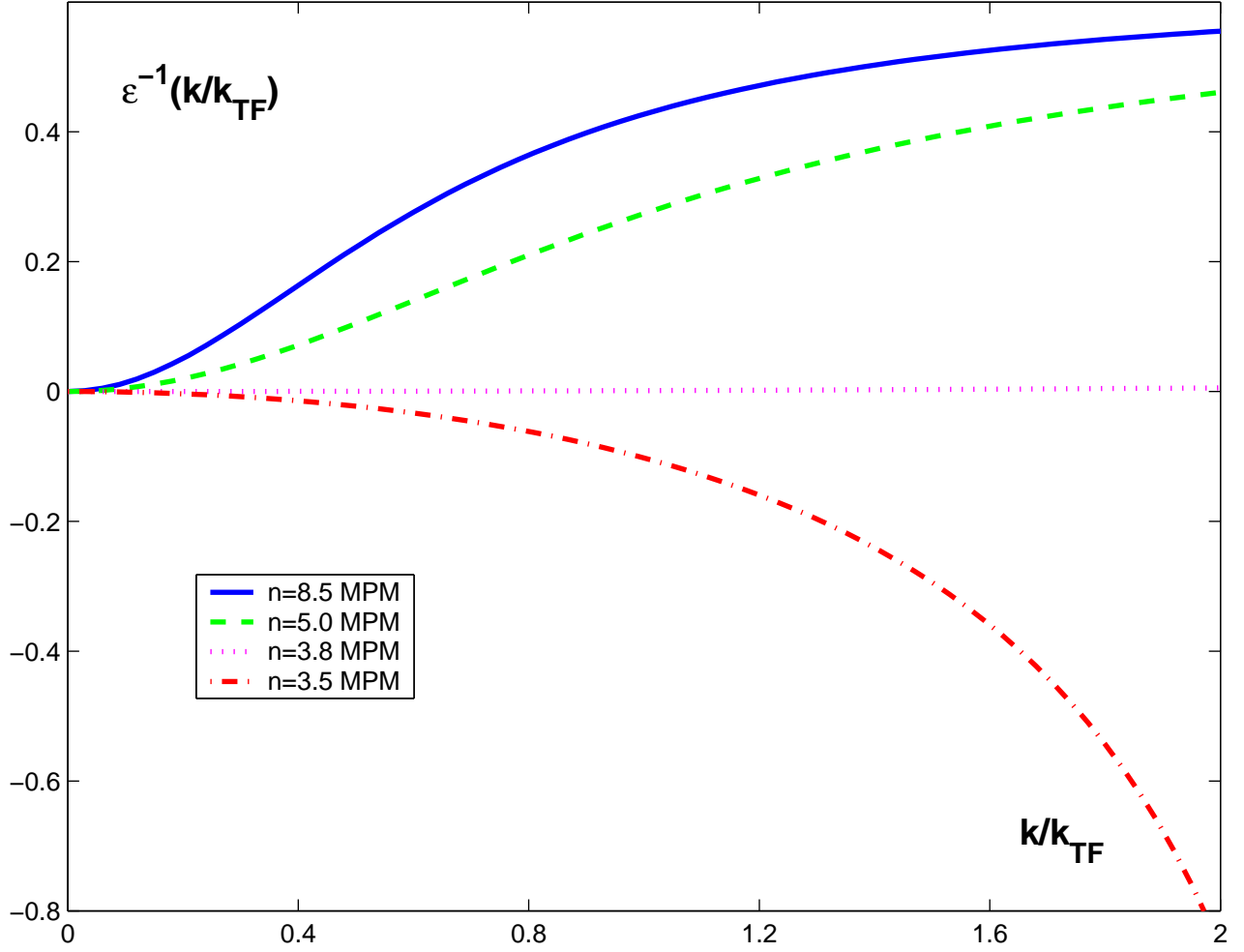


FIG. 6: The inverse static dielectric function $\epsilon^{-1}(k, \omega = 0)$ at various metal concentrations in Li-NH₃ solutions at $T = 240^0$ K (model 2). The values of metal concentration n are indicated at the corresponding lines.

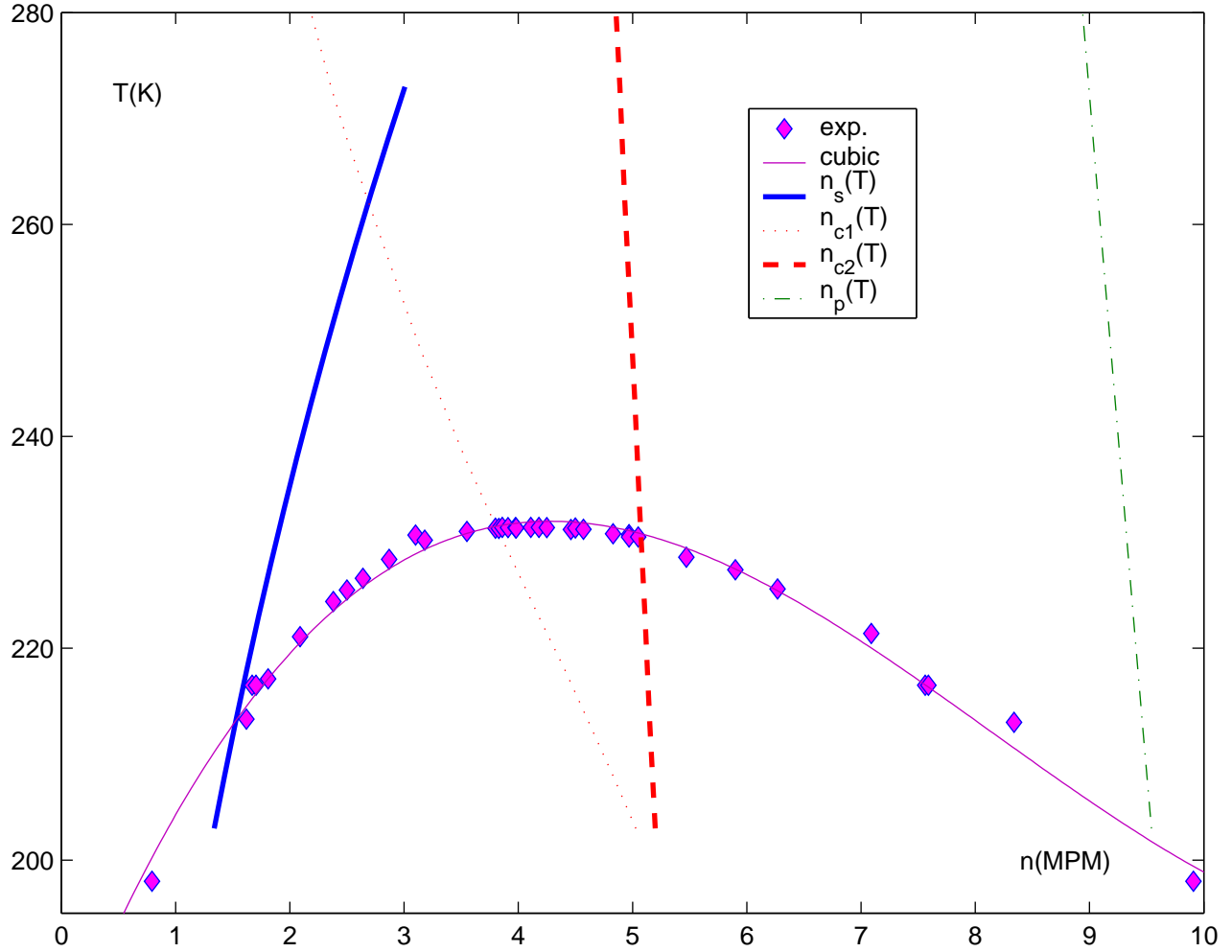


FIG. 7: The phase diagram of the Na-NH₃ solution and the lines of instabilities calculated by model 2. The experimental data^{51,55,56} are indicated by symbols, and their cubic interpolation is indicated by the thick curve. The dotted line corresponds to the polarization catastrophe n_{c1} considered as the onset of metallization. The thin solid line is the low-density spinodal n_s , the dashed one indicates the high-density spinodal n_{c2} , and the dashed-dotted curve yields the zero-pressure line of the pure metallic phase. The bottom of the figure corresponds to the solidification of ammonia.

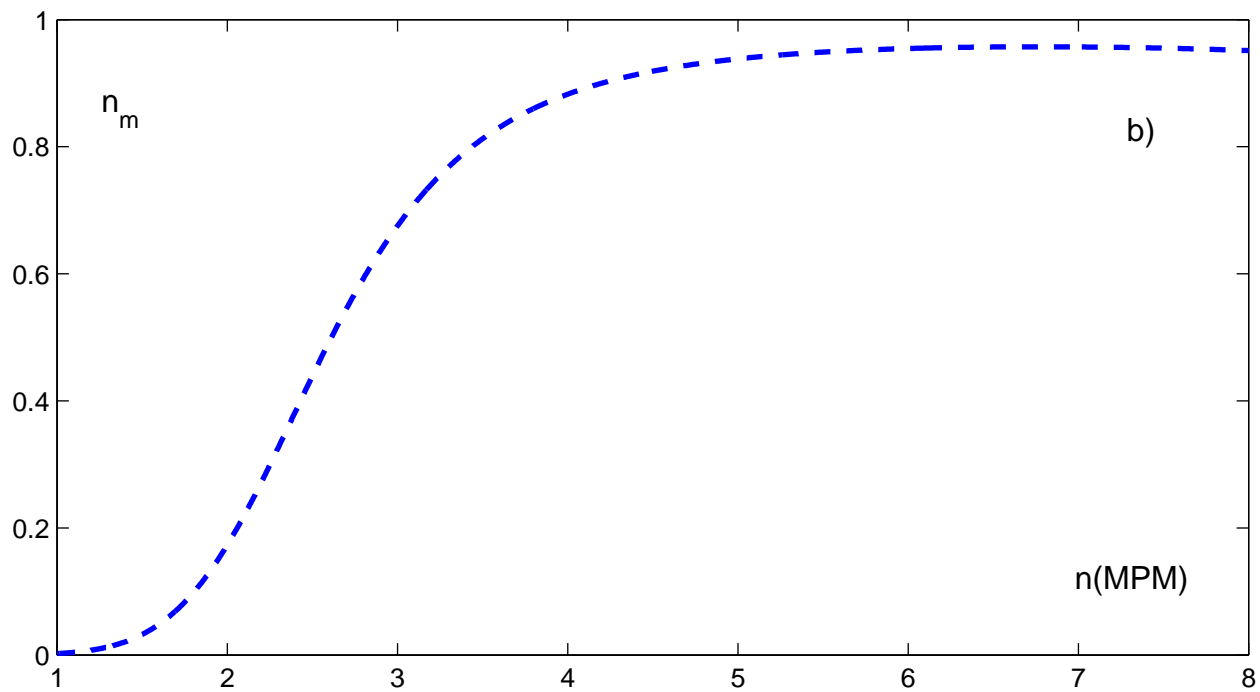
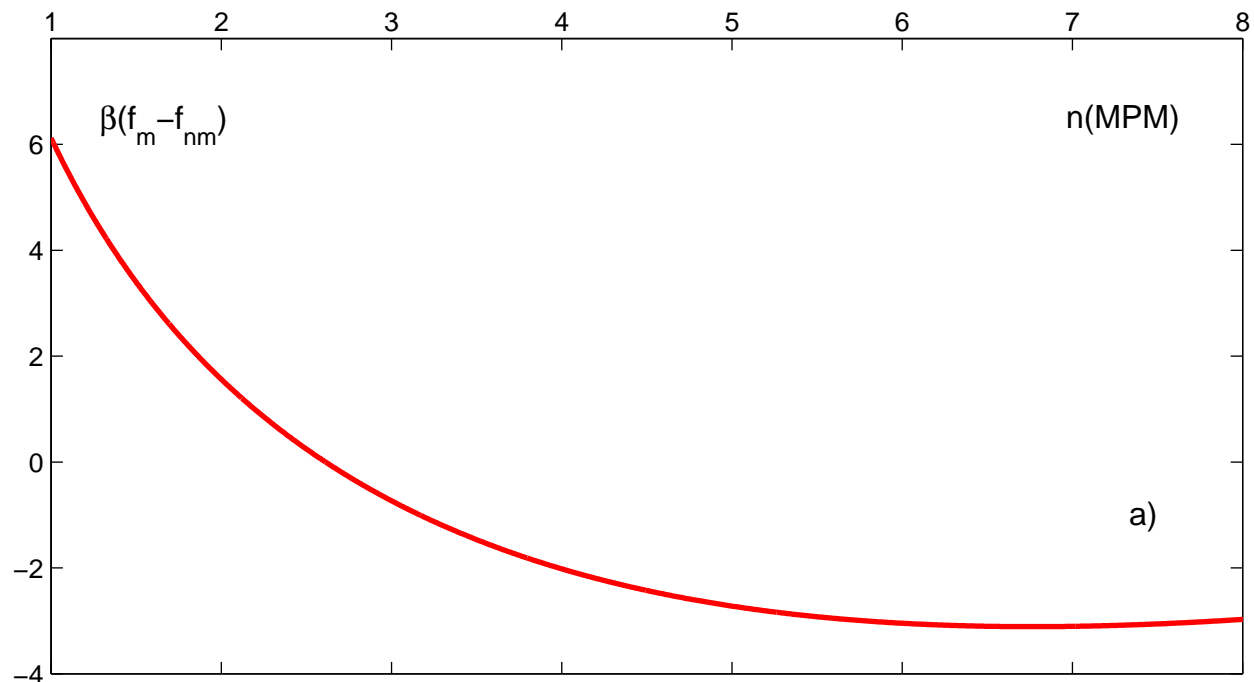


FIG. 8: The dimensionless difference $\beta(f_m - f_{nm})$ in the free energies of metallic and nonmetallic phases (a) and the relative fraction of electrons in delocalized states (b) versus the metal concentration in the Na-NH₃ solution at $T = 240^0\text{K}$, all other parameters of the calculations correspond to Fig. 1.

FIG. 9: Schematic sketch of the influence of thermal fluctuations on the concentration dependencies of the inverse compressibility above (a) and below (b) critical temperature. The dashed-dotted line corresponds to localized electrons, the dashed line represents the inverse compressibility for delocalized electrons. The solid curves correspond to the total inverse compressibility obtained as a sum of the contributions of delocalized and localized electrons, proportionally to their respective densities.

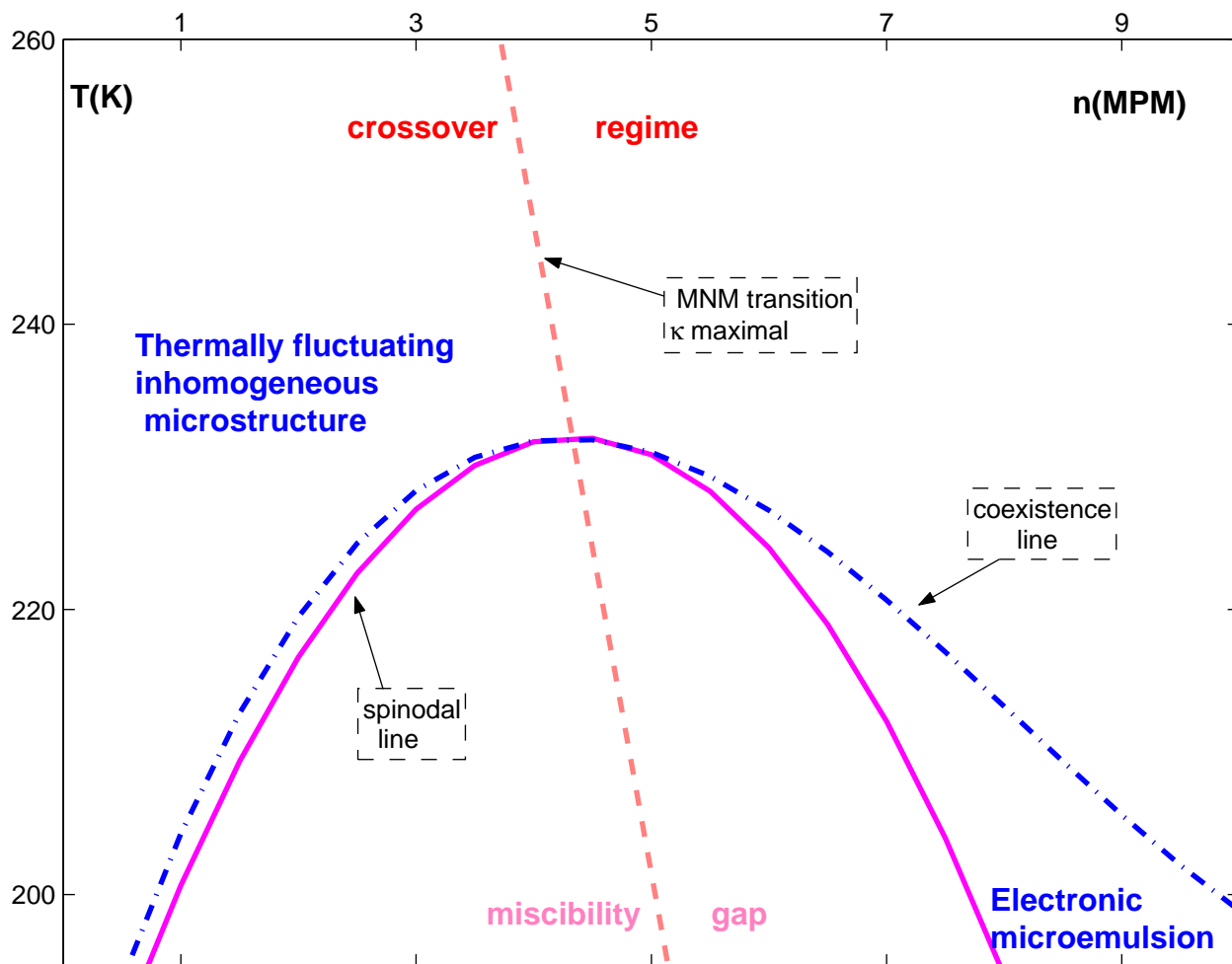


FIG. 10: Schematic sketch of the phase behavior of Na-NH₃ solutions. The dashed line corresponds to the MNM transition, which is attributed to the line of the minimum inverse compressibility. The solid curve is the spinodal line. The dashed-dotted curve corresponds to the line of liquid-liquid coexistence.